ELSEVIER

Chemical Engineering Journal 86 (2002) 243–250

Chemical Engineering Journal

www.elsevier.com/locate/cej

Visualization of 3D gas density distribution using optical tomography

J. Feng [a,*], K. Okamoto [b], D. Tsuru [b], H. Madarame [b], M. Fumizawa [c]

[a] *State Key Laboratory for Novel Software Technology, Department of Computer Science and Technology, Nanjing University, Nanjing 210093, China*
[b] *Nuclear Engineering Research Laboratory, University of Tokyo, Tokai-mura, Ibaraki-ken, Japan*
[c] *Department of High Temperature Engineering, Japan Atomic Energy Research Institute, Tokai-mura, Ibaraki-ken, Japan*

Received 19 May 2000; received in revised form 14 March 2001; accepted 2 May 2001

Abstract

This paper presents a visualization of a 3D gas density distribution, which arose from a safety analysis of a high-temperature gas cooler reactor. The density distribution is reconstructed from holographic interferograms using the techniques of computed tomography. In the reconstruction process, a new reduced bandlimit technique is used in the filtered-backprojection algorithm to deal with the truncated projection data with noise. The results reconstructed from 12 view directions are verified qualitatively by an oxygen molarity detector. It shows that the filtered-backprojection algorithm, integrated with the reduced bandlimit technique, can reconstruct the 3D density distribution from the truncated and noisy projections, and that holographic interferometry is a non-disturbing and powerful tool in flow-visualization for 3D gas flows.

Keywords: Optical tomography; 3D gas density; Filtered-backprojection

1. Introduction

Tomography is a well-developed technique for reconstructing the internal structures of objects from their external transmission or emission projections over different directions. Spatial variation in density can be measured with the variances of refractive index by an interferometer [1].

Exploration of the optical tomography technique in flow-visualization can be traced back over three decades. Matulka and Collins [2] demonstrated the possibility of visualizing an asymmetric 3D density by an optical tomography system with only three directions. During the 1980 and 1990s, progress has been made in both hardware systems and reconstruction [3–5], and applications of optical tomography in flow-visualization continue to appear [6]. Although the optical wavefront sensor [7] is available nowadays, the holographic interferometer, which is a non-disturbing and powerful tool for measuring the gas density distribution in whole volume, is also being studied. The most difficult problem for optical tomography is the lack of sufficient projection data for reconstruction.

Study of gas-exchange flow with diffusion is an important topic in nuclear engineering and nuclear fuel cycle engineering, such as the safety analysis of High-Temperature Engineering Test Reactor [8]. Fumizawa [9] evaluated the exchange-flow rate of helium and air through a small opening. Fumizawa and Okamoto [10] measured the 2D mole fraction distribution of a stably stratified flow using a Mach–Zehnder holographic interferometer. In that study, only 2D flows were studied, because the flow could be assumed to be cylindrically 2D flow. However, it is obvious that the gas-exchange flows are usually complex 3D flows. Information about the 3D density distributions is very important if the exchange process is understood. Therefore, techniques for measuring 3D gas flows are desired. Harauz and Heel [11] exploited exact filters to reconstruct 3D data from 50 projections in random directions. Hesselink [12] studied the 3D density distribution of a helium-air coflow from 36 holographic interferogram projections. However, it is usually difficult to get so many projection data simultaneously. Additionally, when the flow field is relatively large, the interferogram projections may not cover the whole flow field, resulting in truncated projections.

In most applications in engineering, the projections are limited in views, restricted in angle or truncated in length because of considerations of radiation dosage in nuclear engineering, the expense of a 3D laser interferometer system

* Corresponding author. Tel.: +86-25-3593460; fax: +36-25-3594692.
E-mail address: jfeng@nju.edu.cn (J. Feng).

1385-8947/02/$ – see front matter
PII: S1385-8947(01)00185-1

or experimental restrictions. The ill-posed problems can be grouped into two kinds of incomplete projection data: limited views and truncated views. Most reconstruction algorithms in such applications are algebraic reconstruction technique (ART); this is easy to use and the requirements for its iterative procedure are easy to meet. Andersen [13] presented an ART which is better than iterative reconstruction–reprojection. Watt et al. [14] evaluated several ART techniques for reconstruction from six and more projections. Tsuru et al. [15] tried a genetic algorithm based on ART to do reconstruction from eight projections. Youla et al. [16] introduced the concept of projections onto convex sets, and Medoff et al. [17] proposed an operator framework which incorporated a priori information. Verhoeven [18] compared five algorithms: adapted versions of ART, the multiplicative ART, the Gerchberg–Papoulis algorithm, a spectral extrapolation algorithm and the singular-value decomposition technique from limited projection data for physical sciences. One of his conclusions is that reconstruction is better with five views than with 19 at all noise levels with a limited angle of view. In 1996, Feng [19] proposed an optimization approach to try to do reconstruction from only three views for simple, smooth distributions. The two big disadvantages of such iterative algorithms are that they are time-consuming and that errors for distributions may increase after a certain number of iterations, while the errors for the projections keep reducing [14]. The filtered-backprojection algorithm (FBP), which is fast and accurate, is well developed for reconstructing the internal structures of objects from their projections in many applications, such as medical computerized tomography [20]. However, the algorithm implicitly assumes that the number of projections is large enough and that complete projection data are available for every direction without noise. These assumptions are obviously not true in some applications.

There are two reasons which make it possible to develop new algorithms for tomography in engineering rather than adopting the developed algorithms for tomography in diagnostic medicine: algorithms for tomography in engineering are error-tolerable while no error is permitted in diagnostic medicine; the properties or distributions are often smooth, such as the density or temperature of distributions in gas flow with diffusion in flow-visualization, while the structures of objects in diagnostic medicine are discrete.

Besides reconstruction from limited views [21,22], reconstruction from truncated projections is still a challenge. There are several ways to deal with the problem of truncation: estimate the truncated part of the projection by using techniques in sampling [23,24]; recover the truncated part by using prediction from statistics [25] or from Bessel expansions [26], or synthesize a complete projection by preprocessing an ensemble of truncated sets of projections [27]. Muller and Arce [28] analyzed the truncated artifacts which depend on the size and shape of the object projected for the continuous imaging domain.

In this study, the interferogram images of an asymmetric and stable gas-flow field were taken from only 12 view directions. Some of the projections were truncated because of the limit of laser-beam width. In order to reconstruct from the truncated projections, a reduced bandlimit technique is proposed in the Fourier domain. Using the reduced bandlimit technique in FBP algorithm, the 3D gas density distribution was reconstructed.

2. Mach–Zehnder holographic interferometer

Interferometry is a technique that uses a property of waves of light. It compares the shape of a wavefront passing a test section with that of a reference wavefront which does not pass the test section. The difference in wavefront shapes is shown by means of the interference fringes, which are dark and white lines in the interferogram images [29]. A conventional Mach–Zehnder interferometer is one of the holographic interferometers which is usually used for the 2D measurement of gas flows [30].

The intensity in the interferogram, I, has a relation with the difference of integrations of refractive indexes along rays as follows:

$$I = I_0[1 + \cos(2\pi n)] \tag{1}$$

$$n\lambda = K\left[\int_{\text{ray}} \rho(x, y, z)\,\mathrm{d}l - \int_{\text{ray}} \rho_{\text{ref}}(x, y, z)\,\mathrm{d}l\right] = K\int_{\text{ray}} \Delta\rho(x, y, z)\,\mathrm{d}l \tag{2}$$

Here I_0 is the intensity of the laser beam, n the fringe shift at a point, K the Gradstone–Dale constant, λ the wavelength of laser light, ρ the density distribution in the test section, and ρ_{ref} the density distribution in the reference section, which is assumed to be constant, ρ_{air}.

The relation between $\Delta\rho$ and mole fraction of helium, M_{helium}, is

$$M_{\text{helium}} = \frac{\Delta\rho}{\rho_{\text{air}} - \rho_{\text{helium}}} \tag{3}$$

3. Filtered-backprojection algorithm

In the FBP algorithm, a planar cross-section (x, y) at certain z is used. For one view direction at θ, the projection $P_\theta(t)$ is calculated from the fringe shifts in interferogram images:

$$P_\theta(t) = \frac{n\lambda}{K} = \int_{\text{ray}} \Delta\rho(x, y)\,\mathrm{d}l \tag{4}$$

Here $t = x\cos\theta + y\sin\theta$ as shown in Fig. 1:

$$P_\theta(t) = \int_{\text{ray}} \Delta\rho(x, y)\,\mathrm{d}l = \iint_{-\infty}^{\infty} \Delta\rho(x, y)\delta(x\cos\theta + y\sin\theta - t)\,\mathrm{d}x\,\mathrm{d}y \tag{5}$$

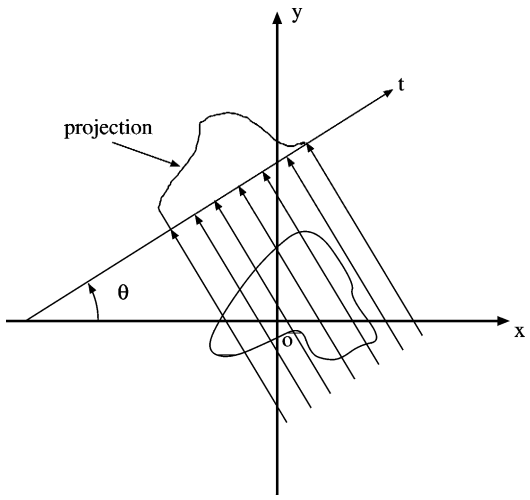

Fig. 1. Configuration of projection on one view direction at θ.

Its Fourier transform is

$$S_\theta(w) = \int_{-\infty}^{\infty} P_\theta(t)\, e^{-jwt}\, dt = \iint_{-\infty}^{\infty} \Delta\rho(x, y)\, e^{-j(xw\cos\theta + yw\sin\theta)}\, dx\, dy \quad (6)$$

Assume

$$G(\omega_1, \omega_2) = \iint_{-\infty}^{\infty} \Delta\rho(x, y)\, e^{-j2\pi(\omega_1 x + \omega_2 y)}\, dx\, dy \quad (7)$$

Using projection slice theorem [31]:

$$S_\theta(\omega) = G(\omega\cos\theta, \omega\sin\theta) = G(\omega, \theta) \quad (8)$$

as well as

$$G(\omega, \theta + \pi) = G(-\omega, \theta) \quad (9)$$

$$h(t) = \int_{-\infty}^{\infty} |\omega|\, e^{j\omega t}\, d\omega \quad (10)$$

we get

$$\Delta\rho(x, y) = \iint_{-\infty}^{\infty} G(\omega_1, \omega_2)\, e^{j2\pi(\omega_1 x + \omega_2 y)}\, d\omega_1\, d\omega_2 = \int_0^{\pi}\int_{-\infty}^{\infty} S_\theta(\omega)|\omega|\, e^{j\omega t}\, d\omega\, d\theta \quad (11)$$

That i:

$$\Delta\rho(x, y) = \int_0^{\pi} \left[\int_{-\infty}^{\infty} P_\theta(\zeta) h(t - \zeta)\, d\zeta\right] d\theta \quad (12)$$

The distribution of $\Delta\rho(x, y)$ at a certain z level is calculated from the function $h(t)$ and the projection $P_\theta(t)$. Then the cross-sections are stacked to form a 3D distribution.

4. Reduced bandlimit for each projection

The function $h(t)$ can be rewritten by making the band-limited projection assumption as follows:

$$h(t) = \int_{-\infty}^{\infty} H(\omega)\, e^{j\omega t}\, d\omega \quad (13)$$

$$H(\omega) = \begin{cases} |\omega| & \text{if } |\omega| < W \\ 0 & \text{otherwise} \end{cases} \quad (14)$$

where W is the maximum frequency, i.e. bandlimit, which is usually half of Nyquist.

In experiments, the projection data may have relatively large noise due to the limitations of image resolution, and they may be truncated in some directions since the laser beam may not be large enough to cover the whole flow field from every direction. In this study, a new technique, the reduced bandlimit, is proposed to deal with those influences.

The influences of truncated projections and noise are assumed to belong mainly to high frequency in the Fourier domain. For the helium–air density stratified flow field, the density distribution has less high spatial frequency because of the molecular diffusion and convection. Therefore, the influences of truncated projections and noise can be reduced by neglecting the high frequency while the density distribution may not be affected. In this study, the bandlimit, W, is searched for each projection in the Fourier domain. The W is determined at which the filtered projection, $[h*P_\theta]$, has less fluctuation. It works like a low-pass frequency filter. On the other hand, the bandlimit W should be as large as possible. Therefore, every projection is assigned a different reduced bandlimit, i.e. reduced bandlimit technique. In processing, a Hamming window is also incorporated for smoothing.

The 3D distribution section is reconstructed using the reduced bandlimit technique with the FBP algorithm.

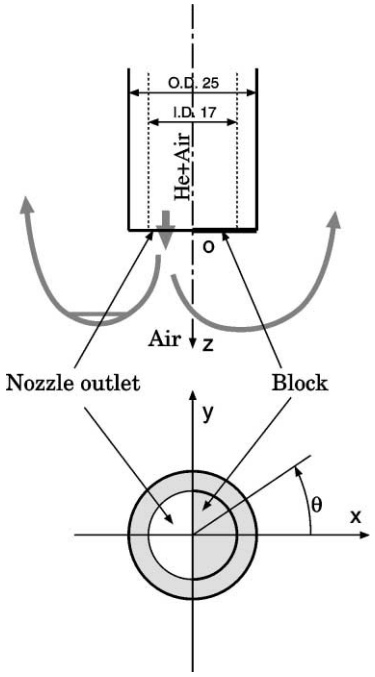

Fig. 2. Configuration of test section and the nozzle.

5. Experiments and processing

5.1. Reconstruction from interferogram image

The steady-state asymmetric flow field is measured using the developed technique. The target is a downward jet of helium–air mixture, gas into air, as shown in Fig. 2. The mole fraction of the mixture gas is 20% helium and 80% air. The downward jet causes a density-stratified flow field, since the density of helium is much less than that of air. The outlet shape of the nozzle is a semi-circle as shown in Fig. 2. Therefore, the density distributions are not two-dimensional. The two-dimensional measurement technique would not be applicable. The outer and inner diameters of the nozzle are 25 and 17 mm, respectively. A half-circle block is attached to the nozzle to form a half-circle outlet. The flow rate of the mixture gas is set to 2ℓ/min (the average velocity is 29.3 cm/s). In this study, the three-dimensional density distributions in the steady stratified flow field are measured. The nozzle can be rotatable in order to obtain many directional views.

A CCD camera is used to record interferograms in 512 × 512 gray images. The images are taken from 12 view directions from 0° to 180° in steps of 15°. The original images of interferograms from 12 view directions are shown in Fig. 3.

With four steps of processing the images—binary, thinning, line segment and fringe shift calculation—2D projection data over 12 views are obtained from 12 interferogram

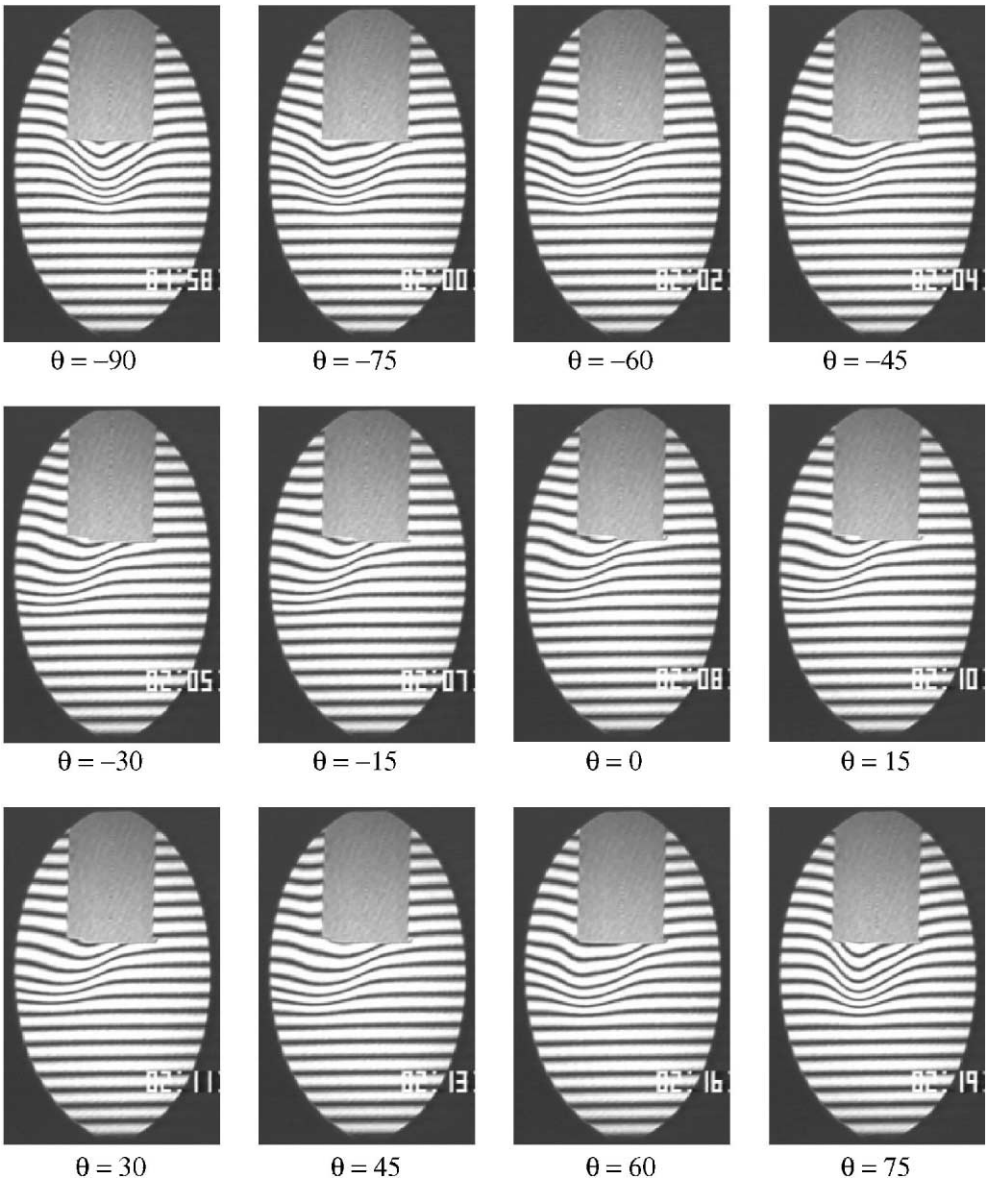

Fig. 3. Images of Interferograms from 12 view directions.

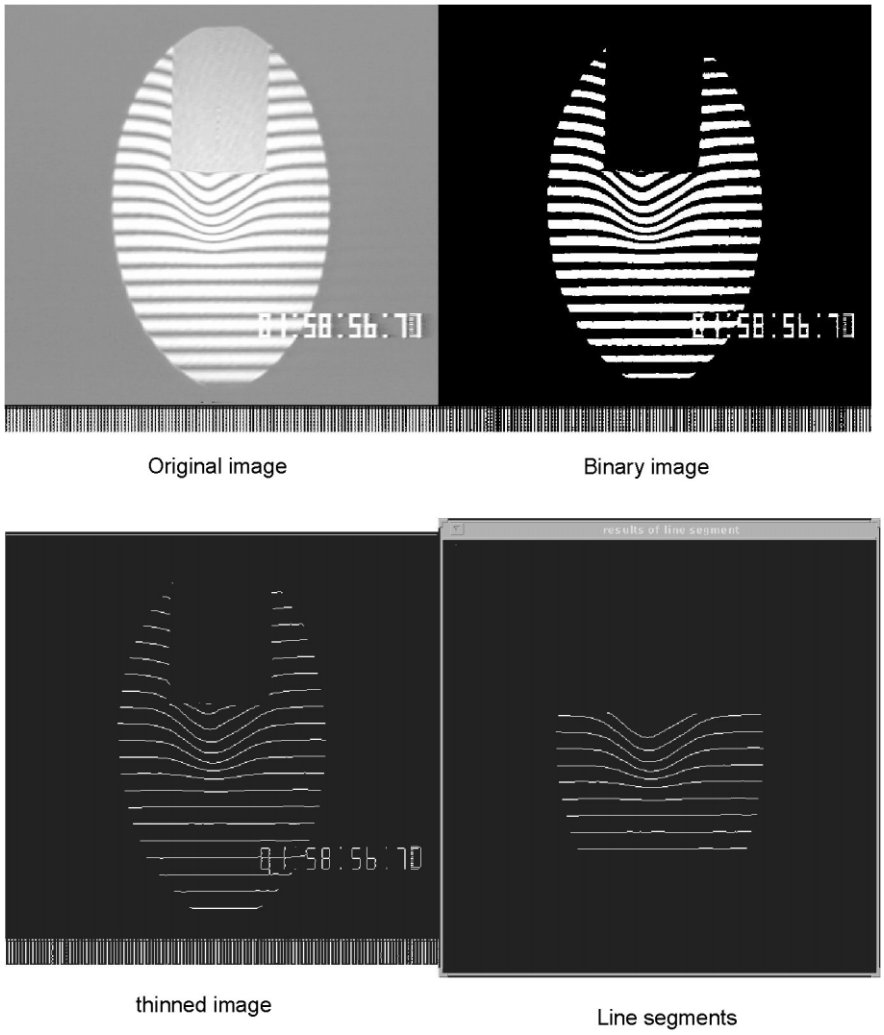

Fig. 4. Image processing for one interferogram.

images as in Fig. 4. The projections on a certain horizontal cross-section are rearranged from the fringe shifts. The projections at certain directions, e.g. $\theta = 0$, are truncated as shown in Fig. 3. Fig. 5 shows two complete and truncated projections and Fig. 6 shows the filtered projections of those in Fig. 5; this shows the effectiveness of the reduced bandlimit technique. Then a density distribution on a cross-section is reconstructed. Finally, the 3D distributions are calculated by stacking the cross-section.

5.2. Verification using oxygen molarity detector

In order to verify the reconstructed 3D density distribution, the densities at several points are measured by an oxygen molarity detector with micro-tube pump. The mole fraction of helium is calculated by using

$$M_{\text{helium}} = 1 - \frac{M_{\text{oxygen}}}{0.2032} \tag{15}$$

The 0.2032 is the mole fraction of oxygen in the air in the experiment. The diameter of the sampling probe is 5 mm, which is relatively large compared with the diameter of the nozzle. Therefore, the measured results may have errors and the probe may disturb the flow itself.

6. Results and discussion

The 3D density distribution in the whole volume of the stratified flow is obtained. Since it is difficult to display the 3D data in two dimensions, several cross-sections of the 3D data are shown. Fig. 7 shows the density distribution of five horizontal cross-sections. Fig. 8 shows the density distribution of two vertical cross-sections passing the center point. These data reveal the 3D density distribution of the stable stratified flow. From the vertical cross-sections at $y = 0$ plane (Fig. 8), the stratified density field can be clearly seen. The downward jet is bent by the effects of the

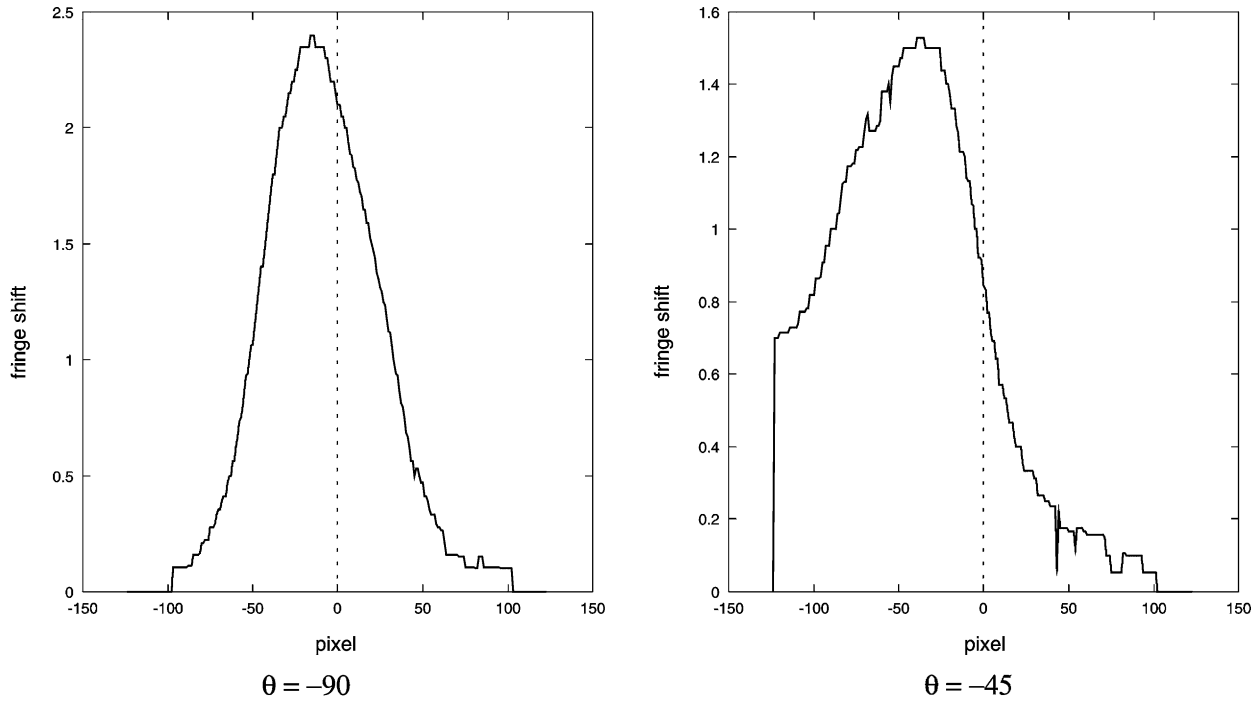

Fig. 5. Two examples of 1D fringe shifts: complete and truncated.

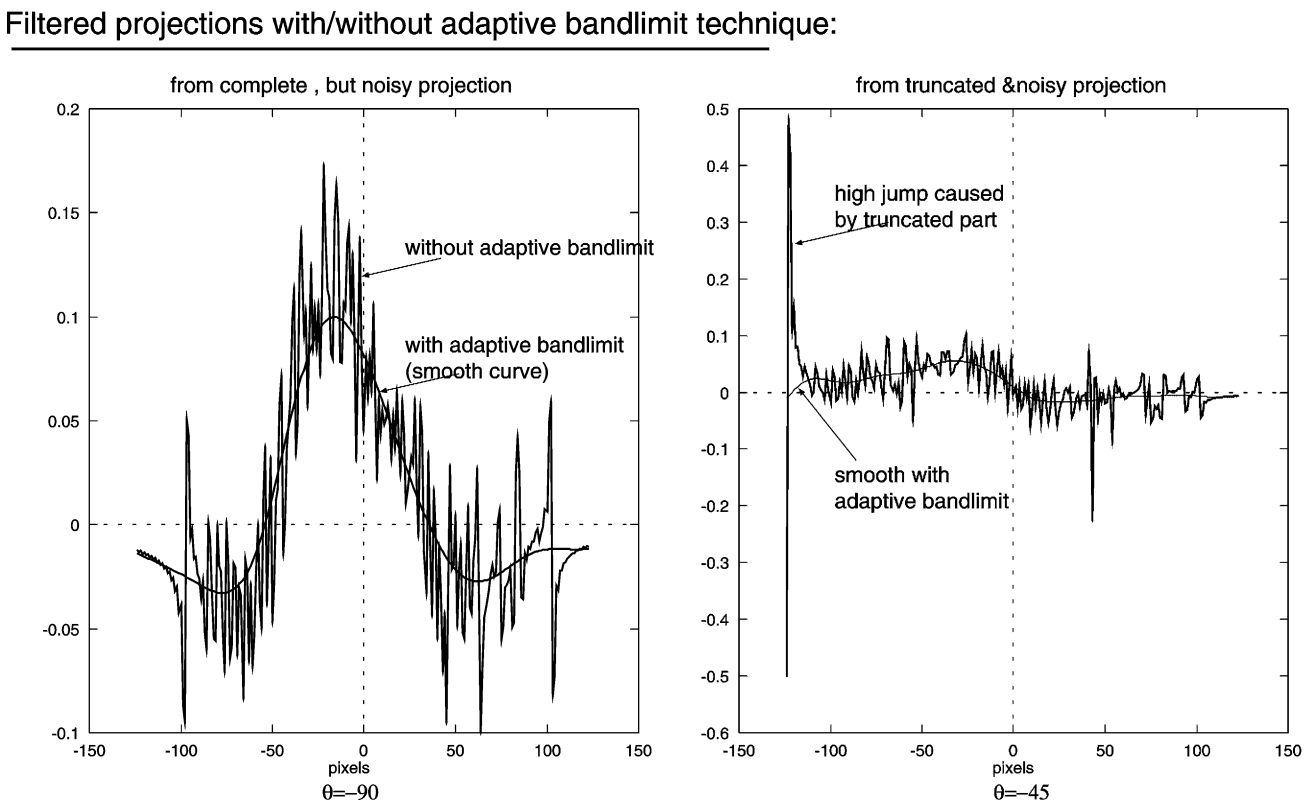

Fig. 6. The effectiveness of the reduced bandlimit (i.e. adaptive bandlimit in the graph) technique.

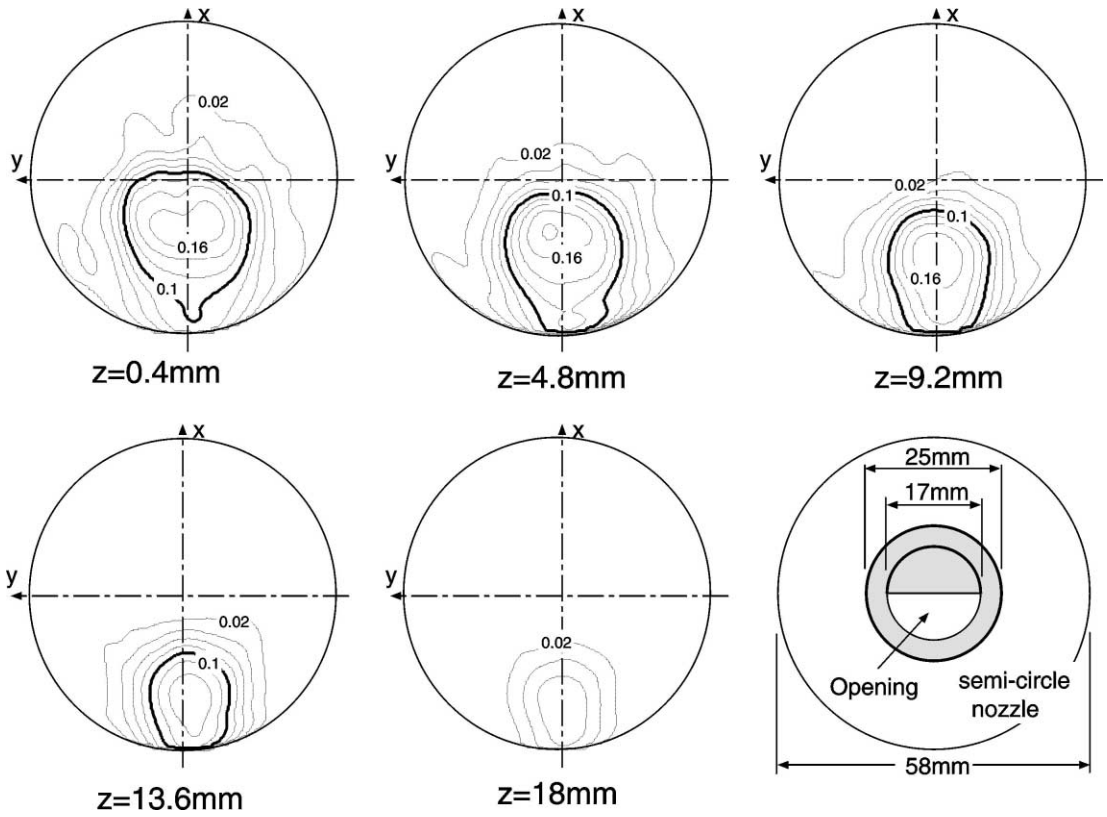

Fig. 7. Contour plots of mole fraction of helium on horizontal cross-sections.

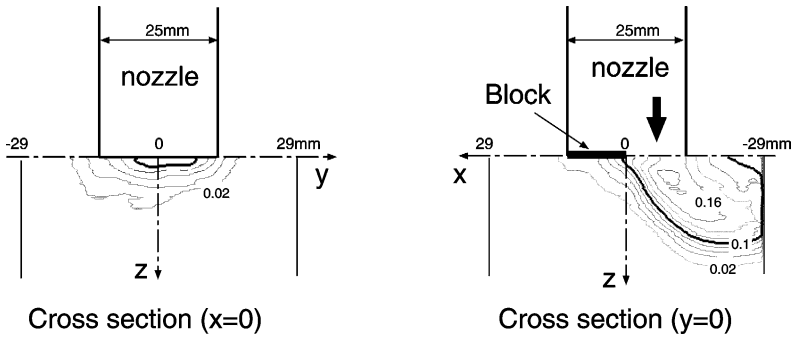

Fig. 8. Contour plots of mole fraction of helium on vertical cross-sections passing zero point.

buoyancy force. From the horizontal cross-sections (Fig. 7), it can be seen that the density distribution is not symmetrical to the *y*-axis. There may be about a 3° inclination between the *x*-axis and the edge of the semi-circle nozzle.

The holographic interferometer does not disturb the flow fields. On the other hand, the test area is limited to a small area where the laser beam passes. The projection data on some view directions may be truncated. Using the reduced bandlimit technique in the FBP algorithm, the influence of the truncated portion can be reduced in the reconstruction of density distributions. Using that technique, the noise can also be reduced.

The reconstructed density distributions are compared with the densities detected by the oxygen meter as shown in Fig. 9. The results measured by the oxygen molarity detector verified qualitatively the reconstructed density distribution. The number of projection data, 12, was thought to be not enough for more accurate results. The reduced bandlimit, which works like a low-pass filter, may also affect the accuracy.

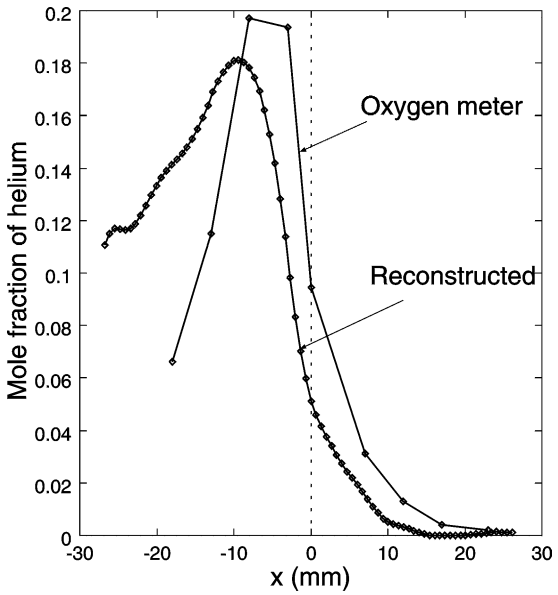

Fig. 9. Comparison of mole fraction of helium along x direction at $z = 4.8\,\text{mm}$, $y = 0\,\text{mm}$.

7. Conclusion

The 3D gas density distribution of a stably stratified flow is measured by using tomography with a holographic interferometer.

To deal with the truncated projections and noise, the new reduced bandlimit technique is applied in the FBP algorithm, which is a proper non-iterative algorithm for real time measuring. The results demonstrate that the reduced bandlimit technique can ignore the high jump aliasing caused by the truncated portion in filtered projections as well as noise. They also show that optical tomography is a powerful tool for measuring 3D gas flows over the whole volume.

Acknowledgements

The authors deeply thank Dr. M. Hishida at JAERI for his helpful discussions and also Mr. T. Hamano for his help in carrying out the experiments.

References

[1] H.-H. Bartels-Lehnhoff, P.H. Baumann, B. Bretthauer, G.E.A. Meier, Computer aided evaluation of interferograms, Exp. Fluids 16 (1993) 46–53.
[2] R.D. Matulka, D.J. Collins, Determination of three-dimensional density fields from holographic interferograms, J. Appl. Phys. 42 (3) (1971) 1109–1119.
[3] H.M. Hertz, Kerr effect tomography for non-intrusive spatially resolved measurements of asymmetric field distributions, Appl. Opt. 25 (1986) 914–921.
[4] W. Faris, R.L. Byer, Quantitative three-dimensional optical tomographic imaging of supersonic flows, Science 238 (1987) 1700–1702.
[5] S.S. Cha, H. Sun, Interferometric tomography of continuous fields with incomplete projections, Opt. Lett. 14 (6) (1989) 299–301.
[6] B.J. Pelliccia-Kraft, D.W. Watt, Three-dimensional imaging of a turbulent jet using shearing interferometry and optical tomography, Exp. Fluids 29 (6) (2000) 573–581.
[7] M.C. Roggeman, B.M. Welsh, P.J. Gardener, R.L. Johnson, B.L. Pedersen, Sensing three-dimensional index-of-refraction variations by means of optical wavefront sensor measurements and tomographic reconstruction, Opt. Eng. 34 (5) (1995) 1374–1384.
[8] JAERI, Present Status of HTGR Research and Development, Tokai-mura, Japan, 1992, pp. 27–30.
[9] M. Fumizawa, Experimental study of helium–air exchange flow through a small opening, Kerntechnik 57 (3) (1992) 156–160.
[10] M. Fumizawa, K. Okamoto, Mole fraction distribution in a slow jet forming a stably stratified field, Kerntechnik 58 (1) (1993) 32–36.
[11] G. Harauz, M.V. Heel, Exact filters for general geometry three-dimensional reconstruction, Optik 73 (4) (1986) 146–156.
[12] L. Hesselink, Optical tomography, in: Handbook of Flow-visualization, Hemisphere, New York, 1989, pp. 307–329.
[13] A.H. Andersen, Algebraic reconstruction in CT from limited views, IEEE Trans. Med. Imag. 8 (1) (1989) 50–55.
[14] D.W. Watt, et al., Computational aspects of optical tomography for fluid mechanics and combustion, ASME-FED 172 (1993) 241–251.
[15] D. Tsuru, et al., Measurement of density distribution using optical tomography with genetic algorithm, FLUCOME'94, 1994, pp. 971–976.
[16] D.C. Youla, et al., Image restoration by the method of convex projections: Part 1—Theory, IEEE Trans. Med. Imag. MI-1 (1982) 81–94.
[17] B.P. Medoff, et al., Iterative convolution backprojection algorithms for image reconstruction from limited data, J. Opt. Soc. Am. 73 (11) (1983) 1493–1500.
[18] D. Verhoeven, Limited-data computed tomography algorithms for the physical sciences, Appl. Opt. 32 (20) (1993) 3736–3754.
[19] J. Feng, Reconstruction in tomography from severe incomplete projection data using multiresolution analysis and optimization, in: Proceedings of the Seventh IEEE Digital Signal Processing Workshop, IEEE, September 1996, pp. 133–136.
[20] A.C. Kak, B.A. Roberts, Reconstruction from projections: applications in computerized tomography, Handbook of Pattern Recognition and Image Processing, Academic Press, New York, 1986.
[21] D.J. Cha, S.S. Cha, Holographic interferometric tomography for limited data reconstruction, AIAA J. 34 (5) (1996) 1019–1026.
[22] J. Feng, S. Bao, Reconstruction of smooth distributions within unsmooth circumferences from limited views using filtered-back-projection algorithm, in 2000 IEEE Nuclear Science Symposium and Medical Imaging Conference Record, IEEE Press, pp. IS-304 to IS–306, 2001.
[23] W. Wagner, Reconstructions from restricted region scan data—new means to reduce the patient dose, IEEE Trans. Nucl. Sci. 26 (1979) 2866–2869.
[24] P.M. Joseph, R.A. Schulz, View sampling requirements in fan beam tomography, Med. Phys. 7 (1980) 692–702.
[25] H. Stark, Image Recovery—Theory and Application, Academic Press, New York, 1987.
[26] D.W. Watt, Fourier–Bessel harmonic expansions for tomography of partially opaque objects, Appl. Opt. 34 (32) (1995) 7468–7473.
[27] M. Muller, G.R. Arce, R.A. Blake, Synthetic scanner arrays in tomographic reconstructions from fan- and cone-beam projections, Appl. Opt. 33 (1994) 8255–8269.
[28] M. Muller, G.R. Arce, Truncation artifacts in tomographic reconstructions from projections, Appl. Opt. 35 (20) (1996) 3902–3914.
[29] M. Philbert, J. Surget, C. Veret, Interferometry, in: Handbook of Flow-visualization, Hemisphere, New York, 1989, pp. 203–210.
[30] W. Merzkirch, The Mach–Zehnder interferometer, in: Flow-visualization, Academic Press, New York, 1974, pp. 102–115.
[31] J. Radon, On the determination of functions from their integrals along certain manifolds, Berchte Saechsische Akademie der Wissenschaften 29 (1917) 262–277.